Inertial-Measurement-Based Catenary Shape Estimation of Underwater Cables for Tethered Robots

Juliette Drupt, Claire Dune, Andrew I. Comport, Sabine Sellier, Vincent Hugel

▶ **To cite this version:**

Juliette Drupt, Claire Dune, Andrew I. Comport, Sabine Sellier, Vincent Hugel. Inertial-Measurement-Based Catenary Shape Estimation of Underwater Cables for Tethered Robots. IEEE/RSJ International Conference on Intelligent Robots and Systems (IROS), Oct 2022, Kyoto, Japan. hal-03841236

HAL Id: hal-03841236
https://hal.science/hal-03841236

Submitted on 28 Nov 2022

HAL is a multi-disciplinary open access archive for the deposit and dissemination of scientific research documents, whether they are published or not. The documents may come from teaching and research institutions in France or abroad, or from public or private research centers.

L'archive ouverte pluridisciplinaire **HAL**, est destinée au dépôt et à la diffusion de documents scientifiques de niveau recherche, publiés ou non, émanant des établissements d'enseignement et de recherche français ou étrangers, des laboratoires publics ou privés.

Inertial-measurement-based catenary shape estimation of underwater cables for tethered robots

Juliette Drupt[1], Claire Dune[1], Andrew I. Comport[2], Sabine Seillier[1], Vincent Hugel[1]

***Abstract*— This paper deals with the estimation of the shape of a catenary for a negatively buoyant cable, connecting a pair of underwater robots in a robot chain. The new estimation method proposed here is based on the calculation of local tangents thanks to the data acquired from inertial measurement units (IMUs), which are attached to the cable near its ends. This method is compared with a vision-based estimation method that was developed previously. Experiments are conducted, in the air and in a pool, using a motion capture system for ground truth. The results obtained show that the new method significantly improves the estimation of the catenary height. Furthermore, the identification of the cable shape is not affected by the limits of the camera's field of view and by the image projection, resulting in increased accuracy and range, without singularities.**

I. Introduction

Underwater real-time communications are limited by the absorption of electromagnetic waves within a few meters. Thus, underwater robots must either be fully autonomous during their missions with no need to communicate in real time (autonomous underwater robots, or AUVs), or be connected to the surface by a physical link allowing control and feedback (remotely operated vehicles, or ROVs). AUVs are mainly used to cover wide areas for missions such as seabed mapping or wreck searching. However, they can only carry out limited tasks, with reduced precision, and cannot properly cope with unexpected situations. ROVs can be teleoperated in order to accomplish tasks that require precision and adaptability. The tether can also provide energy to the ROV for greater autonomy and reduce the ROV's payload thanks to the absence of onboard batteries. Still, the tether limits the mobility of the ROV by involving an energy-intensive drag force, mechanical actions and risks of entanglements. Tether management strategies are therefore crucial to limit these effects and allow exploration in cluttered environments such as caves, flooded mines or shipwrecks.

Such environments require the cable to be shaped to fit into a constrained free space. This can only be achieved by controlling the global shape of the cable itself, which gives rise to a new type of active tether management strategy: the chain of ROVs concept. The idea is to place intermediary robots between the lead ROV and the surface vessel, in order to fully control the 3D shape of the tether between two consecutive robots (Fig. 1). However, it is necessary to estimate the shape of the cable portions along the chain.

This work deals with the 3D shape estimation of a cable portion connecting a pair of underwater robots, which must be robust and precise enough to implement control laws for navigation with obstacle avoidance.

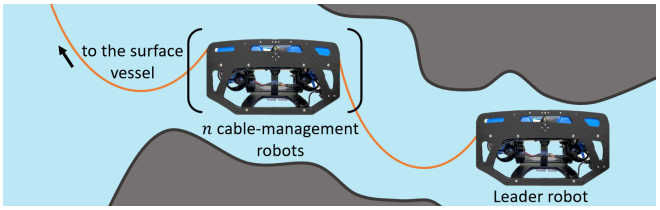

Fig. 1: Chain of ROVs concept

A subsystem of the chain composed of a portion of cable and its robot follower is considered. The solution proposed here is based on the estimation of the tangents at one point or two points of the cable. It only needs the use of two IMUs on the cable near its attachment points.

The contributions of the paper include a new IMU-based catenary shape estimation method, with its implementation on the cable, and a comparison of this method with a previous vision-based estimation method using an underwater motion capture system for ground truth.

Section II introduces the state of the art in matters of tethered robotics and cable shape estimation. Section III describes the system under study, and the two tether shape estimation methods, namely IMU-based and vision-based. Section IV presents the experimental evaluation, and the comparison of both methods on a real system in the air and in a pool. Results are analyzed and discussed before the conclusion in Section V.

II. Related work

Tethered robots can be found in both marine, terrestrial and aerial robotics. In the field of marine robotics, tethers connect underwater robots to the surface or to intermediate vehicles [1], [2] in order to provide real-time communication and, sometimes, energy. The cable can also help to find the robot in case of trouble, especially when exploring confined environments [3]. A stretched tether can allow a terrestrial robot to explore a steep, rugged, and dangerous terrain by clinging it to a fixed support [4]. Robots transporting deformable linear objects can also be assimilated to tethered robots [5], [6]. In addition, a tether can connect parts of a robotic hybrid system, providing communication, power, and the insurance to keep the parts of the system together [7].

Depending on the application and the available computation time, there are different degrees of complexity in the parameterization of cable models. Very simple geometrical

[1]COSMER Laboratory EA7398, Université de Toulon, France
[2]CNRS I3S Laboratory, Université Côte d'Azur, Sophia Antipolis, France

models such as straight 3D lines, if tethers are taut [4], [8], [9], or catenaries if they are slack and heavy enough [10], [11], [6], can be used to describe their shape for real time applications. The catenary model can be derived to take into account the velocity of the cable's end point [12]. In order to consider the dynamics of the cable or the environment, more complex models can be derived with a higher computational cost, such as finite element-based methods [13], [14] or lumped-mass-spring methods [15], [16]. In addition to requiring a prohibitive calculation cost, these models require more information about the environment, such as measures of the water current or parameters of the thrusters, which make them even harder to implement on a real system.

Tethers can be designed as proprioceptive sensors, *e.g.* include an optical fiber [17], [1], [18] or IMUs [19] to estimate their own shape. These solutions allow tracking the shape of a neutrally buoyant tether, however optical fiber shape estimation systems are extremely expensive, and IMU-coated cables cannot be handled properly by winches because of the protrusions the IMUs make on the cable. Furthermore, in both solutions, the longer the cable, the greater the shape estimation error. If the cable is taut, its orientation angles can be measured with an accelerometer placed on the cable [20]. Other solutions do not instrument the tether itself, and use camera feedback. The projection of the cable in the image is often segmented based on a color filter [11], [21], [22]. The cable must be a distinctive color from everything else around it, which is difficult to ensure in an uncontrolled environment. Sim-to-real cable detection learning strategies are proposed to track 2D Bézier curves or splines [23], [24]. Some terrestrial tethered robots are equipped with tension and angle sensors at the cable's end [4]. These measurements are used to detect entanglements and estimate the global 2D shape of the cable, assuming a taut cable, in a framework called T-SLAM [4]. If the cable is managed with a winch, the length of the unfolded cable can be measured and used for estimating and locating the robot [25].

The work described in this paper deals with weighed cables, assuming they can be modeled as catenaries as long as the system is subject to quasi-static movements underwater. The cable itself is not modified, since IMU sensors are simply attached at one end or at both ends of a cable portion that connects two consecutive robots inside the chain. If the cable is to be coiled, then only one of the two ends needs to be equipped with an IMU sensor.

III. Method

A. Notation and coordinate frames

Consider now a subsystem of an underwater robot chain, composed of a robot and the section of cable in front of it. The robot is equipped with a forward camera, an IMU and a water pressure sensor. The cable ends are equipped with two IMUs (Fig. 2).

Let $\mathcal{F}_r$, be the robot frame in SNAME convention. Let P_{a1}, P_{a2} and be the cable attachment points and P_0 the lowest point. By definition, frame $\mathcal{F}_{a1}$ is with origin P_{a1} and axis aligned with $\mathcal{F}_r$, and $\mathcal{F}_0$ is the catenary frame.

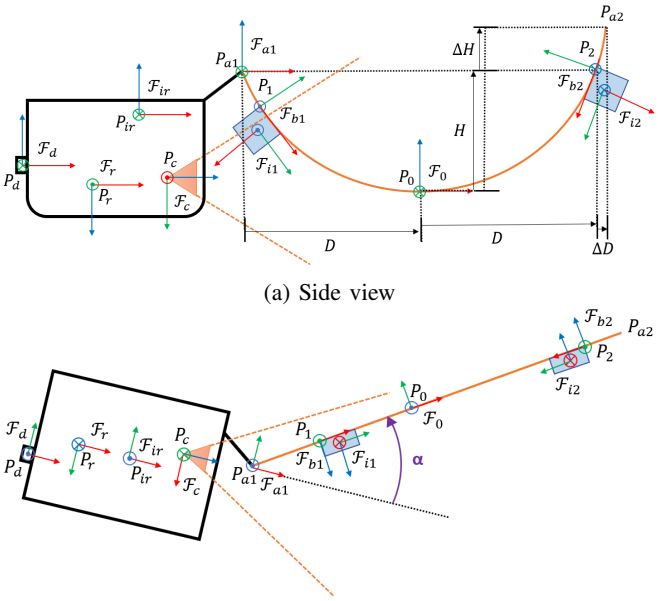

(a) Side view

(b) Top view

Fig. 2: Subsystem composed of a ROV and its front catenary cable with notation, frame definitions, and 3D parameters.

The rotation from $\mathcal{F}_{a1}$ to $\mathcal{F}_0$ is considered to be a pure yaw rotation of magnitude α about the vertical axis. $\mathcal{F}_{ir}$, $\mathcal{F}_{i1}$ and $\mathcal{F}_{i2}$ are robot and cable IMUs' frames, with P_1 and P_2 being the IMUs' fixation points on the cable. $\mathcal{F}_c$ is the camera frame and $\mathcal{F}_d$ the pressure sensor frame. Two additional frames $\mathcal{F}_{b1}$ and $\mathcal{F}_{b2}$ are defined, with respective origins P_1 and P_2, and x-axes tangent to the catenary. IMUs are attached to the cable along this axis, around which the sensor can rotate when the friction of the water on the IMU is strong enough to induce a twist in the cable.

B. Cable modeling

The tether is modeled by a catenary expressed in the $\mathcal{F}_0$ frame, as a function of its length L, the difference in elevation of its attachment points ΔH, and its deflection H:

$$ {}^0Z = \frac{1}{C}[\cosh(C\ {}^0X) - 1] \tag{1} $$

with ${}^0X$ and ${}^0X$ being respectively the coordinates along axis $\mathbf{x}$ and $\mathbf{z}$ of $\mathcal{F}_0$ and where:

$$ C = \frac{2(2H + \Delta H + 2L\sqrt{H\frac{H+\Delta H}{L^2-\Delta H^2}})}{L^2 - (2H + \Delta H)^2} \tag{2} $$

Given a constant length L, the catenary can be fully described in its frame $\mathcal{F}_0$ by H and ΔH. The catenary belongs to a plane perpendicular to $\mathbf{y_0}$ where $\mathbf{y_0}$ is the $\mathbf{y}$ axis of $\mathcal{F}_0$. The addition of the angle α (Fig. 2) between the robot's front axis $\mathbf{x}$ and the plane of the cable completely constrains the subsystem in 3D. The set of parameters to be estimated is then $\{H, \Delta H, \alpha\}$.

C. Parameter estimation

1) ΔH Difference in elevation of attachment points: The depth of P_{a_1} is estimated *via* the water pressure measurement at P_d. The depth measure at P_d is transferred to P_{a_1} thanks to the measurement of the robot orientation given by its IMU.

2) Vision-based estimation: In the vision-based catenary shape estimation [11], assuming zero pitch and roll angles the projection of the catenary is given as:

$$y(a,b,x) = \frac{1}{{}^cZ}[-\frac{\cosh(C\zeta - CD) - 1}{C} + aH_{max} + {}^cY_a] \tag{3}$$

with $a = \frac{H}{H_{max}}$ and $b = \sin(\alpha)$

$$\zeta = \frac{{}^cX_a - x\,{}^cZ_a}{b + x\sqrt{1-b^2}} \tag{4}$$

and

$${}^cZ = \frac{{}^cX_a\sqrt{1-b^2} + b\,{}^cZ_a}{b + x\sqrt{1-b^2}} \tag{5}$$

where $[x, y]^T$ are the coordinates of a point of the cable's projection in the image plane and $[{}^cX_a, {}^cY_a, {}^cZ_a]^T$ the coordinates of P_a in frame $\mathcal{F}_c$. H_{max} is defined arbitrarily as a maximum value allowed for H. Parameter D is represented in Fig. 2.

The cable is segmented in the images by color thresholding. The resulting points are used to estimate the catenary parameters through a Gauss-Newton algorithm that minimizes the function

$$\Gamma(a,b) = \sum_i r_i(a,b)^2 \tag{6}$$

where $r_i(a,b) = y_i - y(a,b,x_i)$.

An *initial guess* (a_0, b_0) is given as input to the optimization algorithm, and corresponds to the catenary whose lowest point P_0 projects in the image plane at the position of the lowest point detected in the image. Due to perspective projection, these points do not match exactly, but they are close enough to make the initial guess consistent. However, if the bottom of the rope moves out of the field of view, the lowest point depth is underestimated.

3) IMU based estimation: In order to improve robustness to vision outliers and numerical optimization singularities, IMU based estimation of the catenary parameters is proposed. It uses three IMUs. One is embedded onboard the robot, and two are fixed on the tether (Fig. 2).

In this case, the yaw angle α is determined from the rotation matrix ${}^rR_{b1}$ or ${}^rR_{b2}$ with:

$${}^rR_{bk} = ({}^wR_{ir}\,{}^{ir}R_r)^T\,{}^wR_{ik}\,{}^{ik}R_{bk}, \quad k \in \{1,2\} \tag{7}$$

where ${}^{ik}R_{bk}$ and ${}^{ir}R_r$ are constant calibrated matrices, and ${}^wR_r$ and ${}^wR_{ik}$ are measured by the robot and the catenary IMUs, respectively.

Figure 3 shows the two cable tangent angles β, at points P_1 and P_2 that are placed at distances L_1 and L_2 from extremities. R_1 is the curvilinear distance along the cable from P_1 to P_0:

$$R_1 = (L - (L_1 + L_2))\frac{g(\beta_1,\beta_2)}{1 + g(\beta_1,\beta_2)} \tag{8}$$

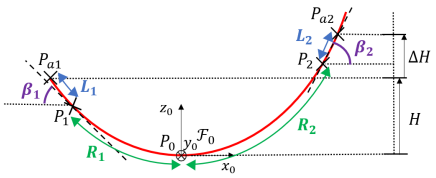

Fig. 3: Introducing catenary tangent angles β_1 and β_2.

with

$$g(\beta_1,\beta_2) = \frac{|tan(\beta_1)|}{|tan(\beta_2)|} \tag{9}$$

The catenary parameter C can be obtained with:

$$C = \frac{1}{R_1}|tan(\beta_1)| \tag{10}$$

Equation 2 is used to recover H as the only positive root of the 2nd degree polynomial $a_2\ H^2 + a_1\ H + a_0 = 0$ where:

$$\begin{aligned} a_2 &= 4C^2(\Delta H^2 - L^2) < 0 \\ a_1 &= 4C(\Delta H^2 - L^2)(C\Delta H + 2) < 0 \\ a_0 &= [C(L^2 - \Delta H^2) - 2\Delta H]^2 > 0 \end{aligned}$$

The catenary parameters can also be estimated with a single tangent, e.g. at P_1 by approximating R_1 with:

$$R_1 = \frac{(L - \Delta H)}{2} - L_1 \tag{11}$$

Symmetrically, R_2 is approximated using the tangent at P_2.

IV. Experiments

A. Robotic system and evaluation metrics

The system is composed of a BlueROV2 tethered to a fixed point by a 1.50 m long 70 g/m red negatively buoyant cable made out of colored ballasted cord (Fig. 7). The robot embeds a camera, an IMU and a water pressure sensor. The cable is equipped with a pair of PhidgetSpatial Precision 3/3/3 High Resolution IMUs, ensuring they did not affect much the visibility of the cable from the embedded camera. The robot and the cable are tracked with a motion capture (mocap) system used in the air and in water.

The following catenary estimation methods are compared and evaluated: i) optimized vision-based (*vision-based optim.*) [11] ii) only vision-based initial guess (*initial-guess*) [11] iii) the proposed IMU-based method (*IMU-based*). Regarding the IMU-based method, the estimation of H is compared with one or both IMUs and the estimation of α using each one of the two cable IMUs separately. *IMU-based-1* refers to using only IMU 1, *IMU-based-2* refers to using only IMU 2, and *IMU-based* refers to using both. Since α estimation implies only one cable IMU, there is no *IMU-based* estimation for this parameter. The mean, median and standard deviation (σ) of the errors on H and α are compared for each method. These errors are denoted e_H and e_α respectively.

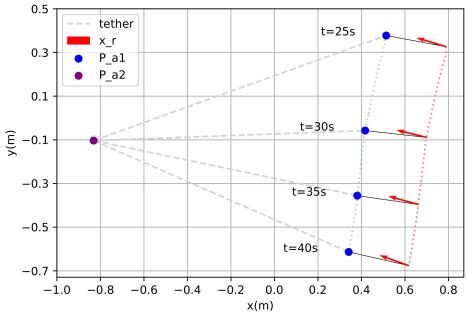

Fig. 4: Trajectory of the robot projected on a horizontal plane. Blue and violet dots represent respectively P_{a1} and P_{a2}. The red arrow is the x axis of $\mathcal{F}_r$. The robot's movement is a composition of a lateral movement and a movement towards P_{a2}.

B. Air configuration

A first series of experiments is set up out of water to test the estimations in a controlled environment where the robot has no pitch or roll, and the system is not disturbed by the hydrodynamics. The statistical analysis is computed on a $117s$ sequence.

The *vision-based optim.* method fails to converge for 11.5 % of the sequence's duration, *i.e.* the optimization does not reach a catenary shape having a sufficiently low cost within the number of allowed iterations. In the following, the results are only evaluated when converged. Figure 4 shows the robot's movements in a representative $15s$ subsequence of the full air sequence. Figure 5 shows H and α parameters estimated by the three methods during the subsequence. While the estimation of α overlaps the ground truth with all methods, the estimation of H by the *vision-based optim.* method shows important errors from $t = 29s$ to $40s$. This coincides with small angles $\alpha \in [-10, 10]$ degrees, *i.e.* one of the singularities where the tether plane is aligned with the optical axis and projects as a line. The error peak of the *initial-guess* method at $t = 37.4s$ is due to an outlier below the tether that shifts the lowest point detection. Figure 6 illustrates *vision-based optim.* and *initial-guess* methods. *IMU-based* methods using only one IMU or both show similar results in the estimation of H in this setup.

TABLE I: Airborne results.

	method	vision optim.	initial guess	IMU 1	IMU 2	both IMUs
e_H (m)	mean	0.0425	0.0165	0.0039	0.0038	**0.0033**
	median	0.0264	0.0312	**0.0022**	0.0031	0.0026
	σ	0.0402	0.0180	0.0131	0.0032	**0.0030**
e_α (°)	mean	2.0331	3.1022	2.7004	**2.0313**	
	median	1.9092	2.8962	2.6741	**1.7106**	x
	σ	1.1038	1.5256	**1.4499**	1.5098	

When considering the whole sequence, all *IMU-based* methods greatly improve the accuracy of H: the error is 5 to 10 times less than the *vision-based optim.* and *initial-guess* estimations (Tab. I).

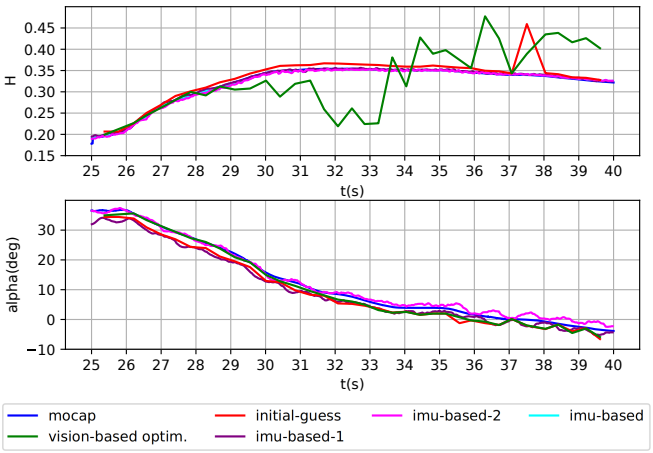

Fig. 5: Estimation of H and α in the air, with fixed ΔH.

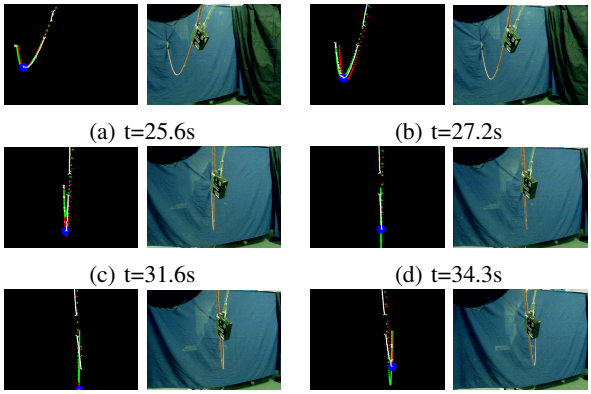

(a) t=25.6s (b) t=27.2s (c) t=31.6s (d) t=34.3s (e) t=37.4s (f) t=39.6s

Fig. 6: Detected cable points (white), with lowest point (blue) and estimated catenary projections for *vision-based optim.* (green) and *initial-guess* (red) methods. Figure 6a shows that both methods give overlapping results. In Fig. 6b, one can observe that the optimization algorithm refines the *initial-guess* result in terms of the reprojection error. Figures 6c, 6d and 6f show examples of bad estimations for *vision-based optim.* when α is close to zero. Figure 6e shows how an outlier below the cable disturbs the *initial-guess* method.

C. Underwater set-up

A similar set-up is deployed in an underwater environment, with an underwater mocap system and the cable's IMUs sealed in waterproof housings (Fig. 7). The following results are based on a $92s$ sequence where the robot pitches and rolls. The hydrodynamic effects and the thrusters' flow distort the catenary model.

The tether moves out of the camera's field of view during 2% of the sequence's duration. In the following, the vision-based methods (*vision-based optim.* and *initial-guess*) are analyzed only when the cable is inside the field of view. 45.3% failure is observed with the *vision-based optim.* method and 0.3% failure with the *initial-guess* method. Figures 8 and 9 respectively show the trajectories applied, and the estimations

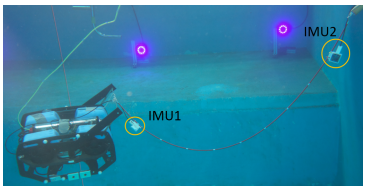

Fig. 7: The system underwater. Optical passive markers are fixed on the robot and on the cable.

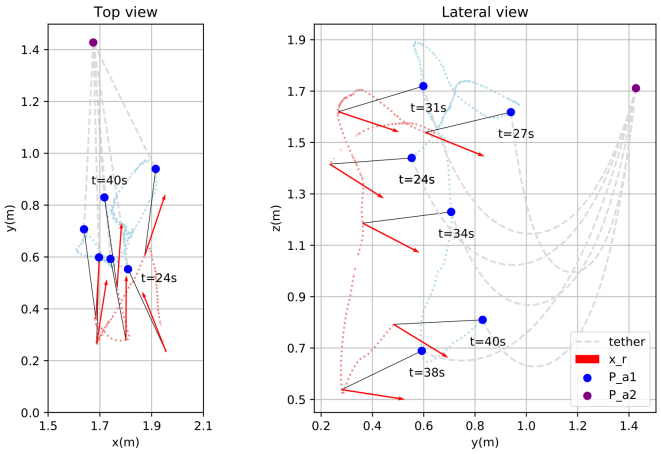

Fig. 8: Trajectory of the robot projected on vertical and horizontal planes. Blue and violet dots represent respectively P_{a1} and P_{a2}. The red arrow is the x axis of $\mathcal{F}_r$. For $t \in [24, 29]$s, the robot moves towards and backwards with yaw variations and minor y, z, roll and pitch variations. For $t \in [19, 40]$s, the robot dives with minor x, y, roll and yaw variations. The robot's pitch changes when diving.

of H and α during a representative sub-sequence. The gaps in the curves correspond to estimation failures. Table II presents a statistical analysis of the full sequence.

TABLE II: Waterborne results.

	method	vision optim.	initial guess	IMU 1	IMU 2	both IMUs
e_H (m)	mean	0.1514	0.1787	0.0835	**0.0333**	0.0438
	median	0.1261	0.1612	0.0621	**0.0299**	0.0406
	σ	0.1188	0.1108	0.0978	**0.0234**	{0.0266
e_α (°)	mean	16.545	16.042	**11.342**	13.270	x
	median	11.030	11.825	**7.7013**	11.013	
	σ	19.655	14.890	**10.608**	10.692	

First, the very important failure rate of the *vision-based optim.* method can be noticed. In the underwater sequence, the color based detection fails at detecting the farthest cable points due to water absorbance, as shown in Fig. 10. Furthermore, the cable projection in the image is deformed with regard to vision based expectations due to roll, pitch, and hydrodynamics, including the currents created by the thrusters. The error in the model makes the vision based optimization fail to fit the cable shape projection properly. The *initial-guess* method gives more robust results with regard to the deformations since it only considers the lowest point. Figure 10 illustrates the behaviour of the *vision-based optim.* and *initial-guess* methods.

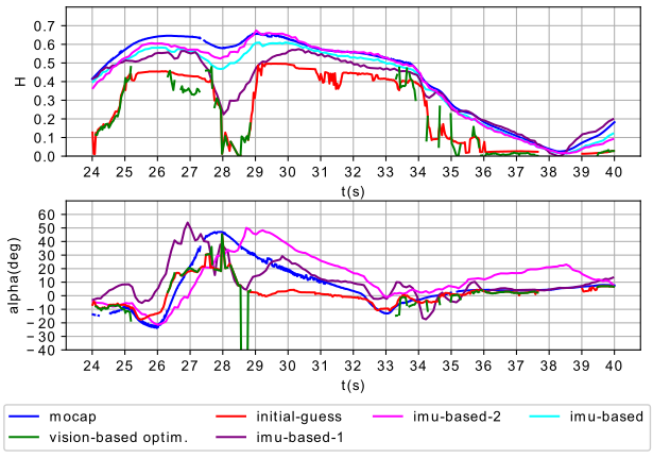

Fig. 9: Estimation of H and α in the pool.

Considering the estimation of H, IMU-based methods perform 3 times better than vision-based methods, and show a smaller dispersion. The estimation from the IMU1 is less accurate due to the thrusters' flow that deforms the rope. For instance, in Fig. 9, one can see an important error for the *IMU-based-1* method at $t \in [27, 29]$s, which coincides with a backwards movement of the robot that propels water onto the IMU1 (Fig. 8).

Looking at α, all methods show similar estimation performances, but with different sources of errors. The *initial-guess* method is impacted by the quality of the tether detection, since it needs the cable's lowest projection point in the image to be properly detected, but this error does not propagate over time. *Vision-based optim.* method suffers from the detection and the deformation of the cable's projection, and eventually shows poor performances compared to the others due to its important failure rate. *IMU-based* methods' errors are partly due to the hydrodynamics of the system, with IMU1 being disturbed by the robot's thrust, and IMU2's movement being impacted by the propagation of the deformations along the cable. There may also be yaw integration issues of IMUs in the absence of a magnetometer, in an indoor environment. During the sequence, the yaw angle was corrected with shift and drift calibration assuming constant drift, which needs to be updated over time. A too sharp motion could also lead to bad yaw integration. In outdoor environments, the method will be more robust thanks to the use of magnetometers.

As a conclusion, it results from this analysis that combining visual and inertial measurements in estimating α could lead to a much more robust estimation of this parameter.

V. Conclusion and Future Work

A new catenary shape estimation approach was introduced for a negatively buoyant underwater cable based on inertial measurements of one or two tangents near the attachment points. This estimation was compared to vision-based estimation from previous work in experiments carried out in the

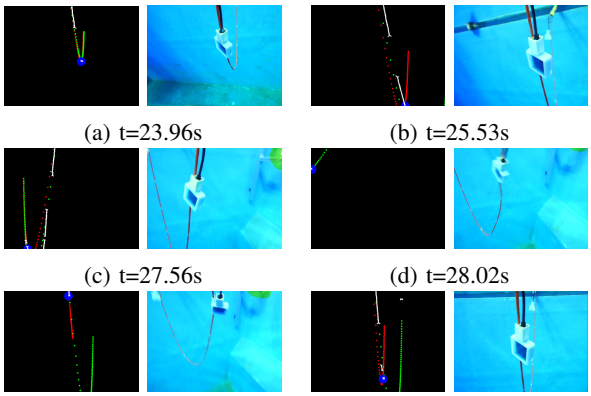

(a) t=23.96s (b) t=25.53s (c) t=27.56s (d) t=28.02s (e) t=28.65s (f) t=33.40s

Fig. 10: Detected tether points (white), with lowest point (blue) and estimated catenary projections for *vision-based optim.* (green) and *initial-guess* (red) methods in the image plane. In Fig. 10a both methods fit the points quite well, whereas in Fig. 10f, the *vision-based optim.* method clearly refines the *initial-guess* in terms of reprojection error. In Figs. 10b, 10d and 10f, the *vision-based optim.* method suffers from the farthest part of the cable not being detected correctly because of color absorption. Figure 10c clearly shows that the deformations of the cable projection in the image make the projection model unsuitable for the *vision-based optim.* and *initial-guess* estimations.

air and in a pool, using a motion tracking system for ground truth. It was shown that the new method is more accurate and robust in estimating the catenary sag. Furthermore, the tested methods can be complementary in estimating the relative cable-robot orientation when the thrusters' flow impacts the IMU orientation. In future works, a fusion between the visual and inertial methods could lead to a much more robust estimation of the cable's orientation.

In addition, the robustness, stability and accuracy of the tether sag estimation make it suitable as a control input to manage the shape of the cable portions inside a chain of robots. Moreover, the estimation gives cable 3D localization information, which can be used to localize the robots relative to each other.

VI. Acknowledgment

This work is funded by the French Research Ministry, the CARTT of the IUT of Toulon. We would like to thank the CEPHISMER of the French Navy for their logistical support.

References

[1] S.-C. Yu, J. Yuh, and J. Kim, "Armless underwater manipulation using a small deployable agent vehicle connected by a smart cable," *Ocean Engineering*, vol. 70, no. 23, pp. 149–159, 2013.

[2] O. Tortorici, C. Anthierens, V. Hugel, and H. Barthelemy, "Towards active self-management of umbilical linking rov and usv for safer submarine missions," in *IFAC-PapersOnline*, vol. 52, no. 21. Daejeon, Republic of Korea: Elsevier, 2019, pp. 265–270.

[3] A. Lasbouygues, S. Louis, B. Ropars, L. Rossi, H. Jourde, H. Délas, P. Balordi, R. Bouchard, M. Dighouth, M. Dugrenot, E. Jacquemin, F. Vasseur, L. Lapierre, and D. Andreu, "Robotic mapping of a karst aquifer," in *IFAC: Int. Federation of Automatic Control*, ser. IFAC WC, Toulouse, France, 2017.

[4] P. McGarey, K. MacTavish, F. Pomerleau, and D. Barfoot, "Tslam: Tethered simultaneous localization and mapping for mobile robots," *The Int. J. of Rob. Research*, vol. 36, no. 12, pp. 1363–1386, 2017.

[5] J. Alonso-Mora, R. Knepper, R. Siegwart, and D. Rus, "Local motion planning for collaborative multi-robot manipulation of deformable objects," in *ICRA*. Seattle, WA, USA: IEEE, 2015, pp. 5495–5502.

[6] D. S. D'Antonio, G. A. Cardona, and D. Saldaña, "The catenary robot: Design and control of a cable propelled by two quadrotors," *IEEE Rob. and Autom. Letters*, vol. 6, no. 2, pp. 3857–3863, 2021.

[7] D. Debruyn, R. Zufferey, S. F. Armanini, C. Winston, A. Farinha, Y. Jin, and M. Kovac, "Medusa: A multi-environment dual-robot for underwater sample acquisition," *IEEE Rob. and Autom. Letters*, vol. 5, no. 3, pp. 4564–4571, 2020.

[8] C. Viel, "Self-management of the umbilical of a rov for underwater exploration," *Ocean Engineering*, vol. 248, p. 110695, Mar. 2022.

[9] ——, "Self-management of ROV umbilical using sliding buoys and stop," *IEEE Rob. and Autom. Letters*, vol. 7, no. 3, pp. 8061–8068, Jul. 2022.

[10] M. Such, J. R. Jimenez-Octavio, A. Carnicero, and O. Lopez-Garcia, "An approach based on the catenary equation to deal with static analysis of three dimensional cable structures," *Engineering Structures*, vol. 31, no. 9, pp. 2162–2170, 2009.

[11] M. Laranjeira, C. Dune, and V. Hugel, "Catenary-based visual servoing for tether shape control between underwater vehicles," *Ocean Engineering*, vol. 200, p. 107018, 2020.

[12] J. Wu, S. Xu, H. Liao, C. Ma, X. Yang, H. Wang, T. Zhang, and X. Han, "Maneuverability and hydrodynamics of a tethered underwater robot based on mixing grid technique," *J. of Marine Science and Engineering*, vol. 9, no. 6, 2021.

[13] N. O.A. and I. Schjølberg, "Finite element cable-model for remotely operated vehicles (rovs) by application of beam theory," *Ocean Engineering*, vol. 163, pp. 322–336, 2018.

[14] Y. Meng, X. Xu, and M. Zhao, "Dynamics calculation of complex deep-sea cable system based on hybrid optimization algorithm," *Ocean Engineering*, vol. 200, p. 107041, 2020.

[15] S. Soylu, B. Buckham, and R. Podhorodeski, "Dynamics and control of tethered underwater-manipulator systems," in *Oceans*. Seattle, WA, USA: MTS/IEEE, 2010, pp. 1—-8.

[16] S. Hong, K. Ha, and J. Kim, "Dynamics modeling and motion simulation of usv/uuv with linked underwater cable," *J. of Marine Science and Engineering*, vol. 8, no. 5, 2020.

[17] R. G. Duncan, M. E. Froggatt, S. T. Kreger, R. J. Seeley, D. K. Gifford, A. K. Sang, and M. S. Wolfe, "High-accuracy fiber-optic shape sensing," in *Sensor Systems and Networks: Phenomena, Technology, and Applications for NDE and Health Monitoring 2007*, K. J. Peters, Ed., vol. 6530, Int. Society for Optics and Photonics. San Diego, CA, USA: SPIE, 2007, pp. 487 – 497.

[18] C. Xu, K. Wan, J. Chen, C. Yao, D. Yan, and C. Wang, "Underwater cable shape detection using shapetape," in *Oceans*. MTS/IEEE, 2016, pp. 1–4.

[19] J. Frank, R. Geiger, D. R. Kraige, and A. Murali, "Smart tether system for underwater navigation and cable shape measurement," 2013, uS Patent 8,437,979.

[20] J.-P. Merlet, "An experimental investigation of extra measurements for solving the direct kinematics of cable-driven parallel robots," in *ICRA*. Brisbane, Australia: IEEE, 2018.

[21] Y. Wu, W. Yan, T. Kurutach, L. Pinto, and P. Abbeel, "Learning to Manipulate Deformable Objects without Demonstrations," in *Proc. of Rob.: Science and Systems*, Corvalis, OR, USA, 2020.

[22] J. Zhu, D. Navarro-Alarcon, R. Passama, and A. Cherubini, "Vision-based Manipulation of Deformable and Rigid Objects Using Subspace Projections of 2D Contours," *Elsevier Rob. and Autonomous Systems*, 2021.

[23] P. Sundaresan, J. Grannen, B. Thananjeyan, A. Balakrishna, M. Laskey, K. Stone, J. E. Gonzalez, and K. Goldberg, "Learning rope manipulation policies using dense object descriptors trained on synthetic depth data," in *ICRA*. IEEE, 2020.

[24] M. Yan, Y. Zhu, N. Jin, and J. Bohg, "Self-supervised learning of state estimation for manipulating deformable linear objects," *IEEE Rob. and Autom. Letters*, vol. 5, no. 2, pp. 2372–2379, 2020.

[25] A. C. Murtra and J. M. Mirats-Tur, "Imu and cable encoder data fusion for in-pipe mobile robot localization," in *Conf. on Technologies for Practical Robot Applications (TePRA)*. Woburn, MA, USA: IEEE, 2013, pp. 1–6.